scientific reports

Check for updates

OPEN

Explore how immobilization strategies affected immunosensor performance by comparing four methods for antibody immobilization on electrode surfaces

Jiaoling Huang, Zhixun Xie✉, Liji Xie, Sisi Luo, Tingting Zeng, Yanfang Zhang, Minxiu Zhang, Sheng Wang, Meng Li, You Wei, Qing Fan, Zhiqin Xie, Xianwen Deng & Dan Li

Among the common methods used for antibody immobilization on electrode surfaces, which is the best available option for immunosensor fabrication? To answer this question, we first used graphene-chitosan-Au/Pt nanoparticle (G-Chi-Au/PtNP) nanocomposites to modify a gold electrode (GE). Second, avian reovirus monoclonal antibody (ARV/MAb) was immobilized on the GE surface by using four common methods, which included glutaraldehyde (Glu), 1-ethyl-3-(3-dimethylaminopropyl)-carbodiimide/*N*-hydroxysuccinimide (EDC/NHS), direct incubation or cysteamine hydrochloride (CH). Third, the electrodes were incubated with bovine serum albumin, four different avian reovirus (ARV) immunosensors were obtained. Last, the four ARV immunosensors were used to detect ARV. The results showed that the ARV immunosensors immobilized via Glu, EDC/NHS, direct incubation or CH showed detection limits of $10^{0.63}$ EID_{50} mL^{-1}, $10^{0.48}$ EID_{50} mL^{-1}, $10^{0.37}$ EID_{50} mL^{-1} and $10^{0.46}$ EID_{50} mL^{-1} ARV (S/N = 3) and quantification limits of $10^{1.15}$ EID_{50} mL^{-1}, and $10^{1.00}$ EID_{50} mL^{-1}, $10^{0.89}$ EID_{50} mL^{-1} and $10^{0.98}$ EID_{50} mL^{-1} ARV (S/N = 10), respectively, while the linear range of the immunosensor immobilized via CH (0–$10^{5.82}$ EID_{50} mL^{-1} ARV) was 10 times broader than that of the immunosensor immobilized via direct incubation (0–$10^{4.82}$ EID_{50} mL^{-1} ARV) and 100 times broader than those of the immunosensors immobilized via Glu (0–$10^{3.82}$ EID_{50} mL^{-1} ARV) or EDC/NHS (0–$10^{3.82}$ EID_{50} mL^{-1} ARV). And the four immunosensors showed excellent selectivity, reproducibility and stability.

Electrochemical immunosensors are a novel detection method that are combined with electrochemical analysis and immunoassays and are widely used in the diagnosis of various pathogens due to their advantages of simplicity, rapidity, and high sensitivity in point-of-care testing[1,2]. The sensitivity and linear range of electrochemical immunosensors are affected by the electrode surface modification and antibody immobilization strategy[3,4]. Electrochemical immunosensors can be categorized as "label-free" and "sandwich" types[5,6]. "Sandwich" immunosensors waste time and energy compared to the "label-free" type, in which the electrochemical signal molecule is immobilized on the electrode or dissolved in an electrolyte in only one step to detect the target[7,8]. Therefore, it is more desirable to construct "label-free" electrochemical immunosensors.

Substrate materials with large specific surface areas and high conductivities are important in improving the capabilities of electrochemical immunosensors. The large specific surface area enhances antibody surface loading[9], and the high conductivity enhances electron transfer from the target molecules to the surface of electrode[10]. Different nanoparticles with large specific surface areas and high electronic transmission capabilities were used to modify electrode surfaces and to increase the sensitivity and linear range of "label-free" electrochemical immunosensors, and this approach has been reported many times[11,12]. Graphene (G) has shown

Guangxi Key Laboratory of Veterinary Biotechnology, Key Laboratory of China (Guangxi)-ASEAN Cross-Border Animal Disease Prevention and Control, Ministry of Agriculture and Rural Affairs of China, Guangxi Veterinary Research Institute, Nanning, Guangxi, China. ✉email: xiezhixun@126.com

potential for application in electrochemical immunosensors because of its low manufacturing cost, superior conductivity and large specific surface area[13]. Among metal nanomaterials, gold nanoparticles (AuNPs) and platinum nanoparticles (PtNPs) are most widely used in electrochemical immunosensors because of their excellent performance and excellent conductivity[14,15]. Additionally, G has been functionalized and adsorbed on chitosan (Chi) through π–π stacking to form graphene-chitosan (G-Chi) hybrid materials[16]. In the G-Chi hybrid materials, Chi chelates Au^{3+} and Pt^{2+} metal ions and acts as a reducing agent to convert the Au^{3+} and Pt^{2+} ions into AuNPs and PtNPs[17,18]; further, G-Chi hybrid materials can be loaded with substantial amounts of AuNPs and PtNPs because of the large specific surface area of G. Hence, we designed a "label-free" electrochemical immunosensor based on G-Chi-Au/PtNP nanocomposites in this work.

In addition, effective immobilization of antibodies is an essential step in constructing electrochemical immunosensors and constitute another important factor in improving the performance of the electrochemical immunosensors[19]. The sensitivities and linear ranges of electrochemical immunosensors are limited by the antibody immobilization strategy chosen[20]. Various antibody immobilization strategies, including glutaraldehyde (Glu) cross-linking, 1-ethyl-3-(3-dimethylaminopropyl)-carbodiimide/*N*-hydroxysuccinimide (EDC/NHS) chemistry, direct incubation and cysteamine hydrochloride (CH), have been exploited by different research groups[21–26], but it is not known which approach is best. To answer this question, four immobilization strategies were compared in the present study: (1) Glu immobilization, (2) EDC/NHS immobilization, (3) direct immobilization and (4) CH immobilization. The results showed that the linear range obtained with the CH immobilization strategy was 10 times broader than that realized with the direct immobilization strategy and 100 times broader than those seen with the Glu immobilization strategy and EDC/NHS immobilization strategy, and their detection limits were similar.

Results and discussion

Nanoparticle synthesis and characterization. A transmission electron microscopy (TEM) micrograph of G-Chi, which has a thin, wrinkled, rippled and flake-like structure, is shown in Fig. 1a. Figure 1b shows the TEM micrograph of G-Chi-Au/PtNP, which indicates that Au/Pt was loaded on the surface of G-Chi. In addition, energy dispersive spectroscopy (EDS) elemental analysis of G-Chi-Au/PtNP was employed to determine the presence of Au and Pt, which confirmed that Au/PtNP had been loaded on the surface of G-Chi (Fig. 1c). The mechanism for formation of G-Chi-Au/PtNP involved Au^{3+} and Pt^{2+} adsorption from aqueous solution due to chelation by G-Chi and then reduction to Au/Pt nanoparticles by Chi. Chi was used as both a stabilizing agent and reducing agent.

Electrochemical characterization. Electrochemical impedance spectroscopy (EIS) is an effective technique for probing the features of surface modified electrodes, and it sensitively analyzes the interactions of analytes with modified electrodes and produces measurable electric signals. More important, EIS is more sensitive than either amperometric or voltammetric methods[27,28]. In typical EIS Nyquist plots, a semicircle appears in the high-frequency region, while a line appears in the low-frequency region, and the diameter of the semicircle corresponds to the electron transfer resistance (R_{et}). In brief, the resistance on the surface of the electrode can be estimated by determining the semicircle diameter. Here, EIS was employed to characterize which material is better for electrode modification, and the results are shown in Fig. 2. The diameter of the semicircle in the Nyquist plot of GE corresponds to an impedance of 1561 Ω, which was decreased to 1167 Ω, 950 Ω and 439 Ω upon modification of the GE with G-Chi-PtNP, G-Chi-AuNP, and G-Chi-Au/PtNP, respectively, due to the high conductivities of G, AuNP and PtNP. These results showed that G-Chi-Au/PtNP exhibited the fastest electron transfer, and it was selected as the material for GE modification.

In addition, EIS was employed to survey the layer-by-layer modification of GE. Figure 3a and f shows that after the ARV/MAb was immobilized on GE-G-Chi-Au/PtNP by four different methods, the R_{et}s of the GE-G-Chi-Au/PtNP-Glu-ARV/MAb, GE-G-Chi-Au/PtNP-ARV/MAb, GE-G-Chi-Au/PtNP-EDC/NHS-ARV/MAb and GE-G-Chi-Au/PtNP-CH-ARV/MAb increased to 965 Ω, 1232 Ω, 1519 Ω and 1778 Ω, respectively, because ARV/MAb is protein with poor electrical conductivity and impedes electron transfer to the surface of the electrode. After GE-G-Chi-Au/PtNP-Glu-ARV/MAb, GE-G-Chi-Au/PtNP-ARV/MAb, GE-G-Chi-Au/PtNP-EDC/NHS-ARV/MAb and GE-G-Chi-Au/PtNP-CH-ARV/MAb were blocked with BSA, their R_{et} values were further increased to 1598 Ω, 2078 Ω, 2331 Ω and 2670 Ω, respectively (Fig. 3b,f), because BSA is a protein. More important, these results show that the ability of the four different methods for ARV/MAb immobilization decreased in the order CH > EDC/NHS > direct incubation > Glu. After GE-G-Chi-Au/PtNP-Glu-ARV/MAb-BSA, GE-G-Chi-Au/PtNP-ARV/MAb-BSA, GE-G-Chi-Au/PtNP-EDC/NHS-ARV/MAb-BSA and GE-G-Chi-Au/PtNP-CH-ARV/MAb-BSA were incubated with $10^{6.82}$ EID_{50} mL^{-1} ARV, the ARV was adsorbed on the electrodes via a specific response with ARV/MAb, and the corresponding R_{et}s were further increased to 4841 Ω, 7468 Ω, 5547 Ω, and 9417 Ω (Fig. 3c,f) because electron transfer to the surface of the electrode was impeded by the ARV protein, and the results demonstrated that the ability of the four different immunosensors to combine ARV decreased in the order CH > direct incubation > EDC/NHS > Glu. Most importantly, the different relative orders for ARV/MAb immobilization and the ARV immobilization demonstrated that the number of ARVs adsorbed on the immunosensors was not only related to the number of ARVs/MAbs but was also affected by the method used to immobilize the ARVs/MAbs.

In addition, BSA was immobilized on GE-G-Chi-Au/PtNP by four different methods to evaluate the ability of the four methods to immobilize protein again, the results are shown in Fig. 3d and f. The R_{et}s of the GE-G-Chi-Au/PtNP-Glu-BSA, GE-G-Chi-Au/PtNP-BSA, GE-G-Chi-Au/PtNP-EDC/NHS-BSA and GE-G-Chi-Au/PtNP-CH-BSA were increased to 1196 Ω, 1613 Ω, 2159 Ω and 2537 Ω because the BSA protein adsorbed on the surface of GE-G-Chi-Au/PtNP impeded electron transfer to the surface of the electrode. These results showed

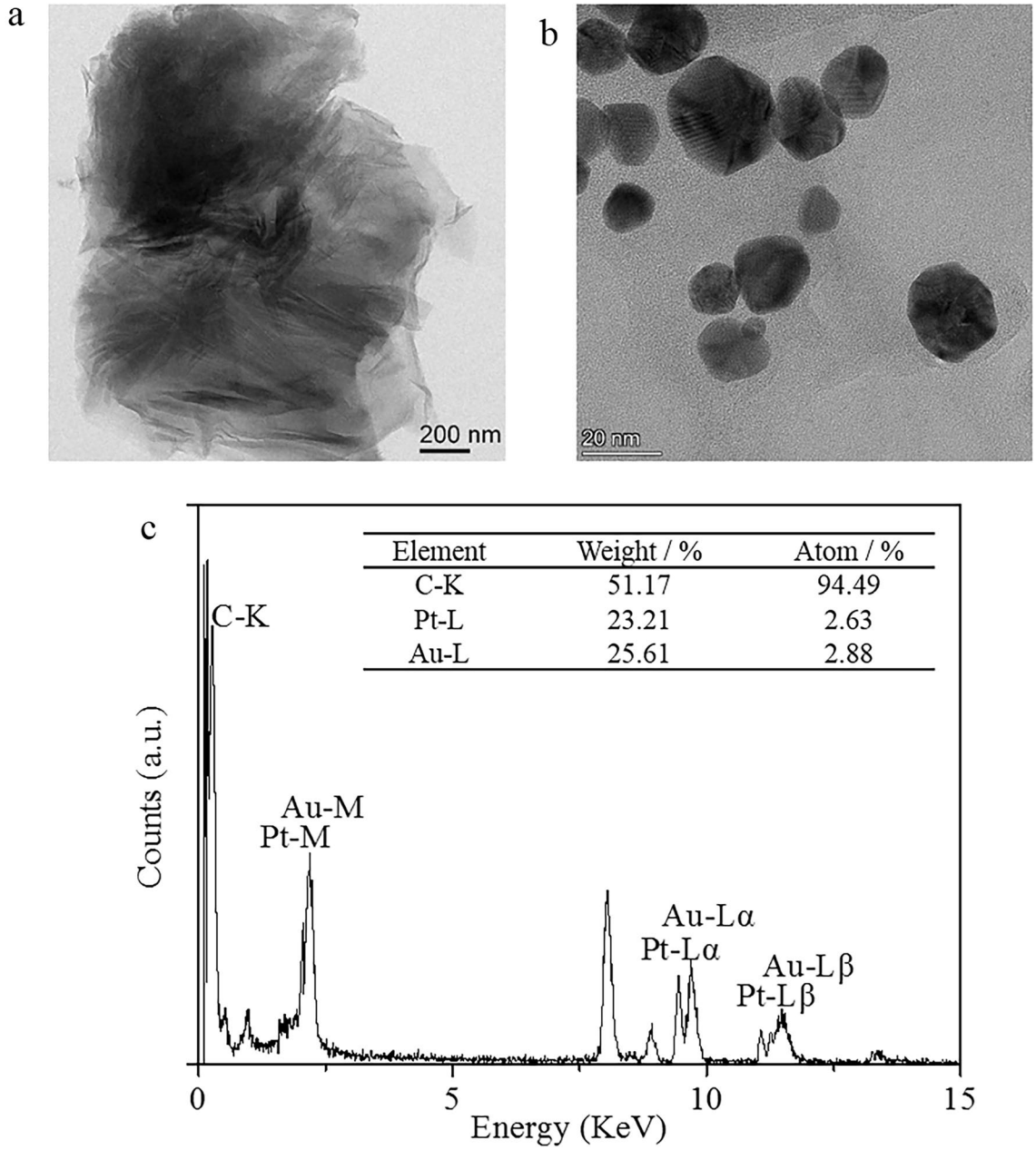

Figure 1. Characterization of the investigated nanocomposites. TEM images of G-Chi (**a**) and G-Chi-Au/PtNP (**b**). EDS elemental analysis of G-Chi-Au/PtNP (**c**).

that the abilities of the four different methods to immobilize BSA decreased in the order CH > EDC/NHS > direct incubation > Glu, which corresponds to the results for ARV/MAb immobilization on GE-G-Chi-Au/PtNP by the four different methods. To evaluate the specificities of the immunosensors, GE-G-Chi-Au/PtNP-Glu-BSA, GE-G-Chi-Au/PtNP-BSA, GE-G-Chi-Au/PtNP-EDC/NHS-BSA and GE-G-Chi-Au/PtNP-CH-BSA (which were not yet immobilized with ARV/MAb) were incubated with $10^{6.82}$ EID_{50} mL^{-1} ARV, the results were showed in Fig. 3e and f. The results showed that the values of R_{et}s of GE-G-Chi-Au/PtNP-Glu-BSA, GE-G-Chi-Au/PtNP-BSA, GE-G-Chi-Au/PtNP-EDC/NHS-BSA and GE-G-Chi-Au/PtNP-CH-BSA were hardly change after incubation with ARV, which suggested that the GE-G-Chi-Au/PtNP-Glu-ARV/MAb-BSA, GE-G-Chi-Au/PtNP-ARV/MAb-BSA, GE-G-Chi-Au/PtNP-EDC/NHS-ARV/MAb-BSA and GE-G-Chi-Au/PtNP-CH-ARV/MAb-BSA had high specificities.

Sensitivity, saturation and extended dynamic range are important factors used to evaluate the performance of an immunosensor. To obtain this information for the immunosensors, the GE-G-Chi-Au/PtNP-Glu-ARV/MAb-BSA, GE-G-Chi-Au/PtNP-EDC/NHS-ARV/MAb-BSA, GE-G-Chi-Au/PtNP-ARV/MAb-BSA and GE-G-Chi-Au/PtNP-CH-ARV/MAb-BSA were used to detect ARV at a concentration of $10^{6.82}$ EID_{50} mL^{-1} to $10^{0.82}$ EID_{50} mL^{-1}. The results are shown in Fig. 4. R_{et} increased with increasing concentrations of ARV due to the increased formation of the antigen–antibody complex, which is a nonconducting biomolecule. As observed,

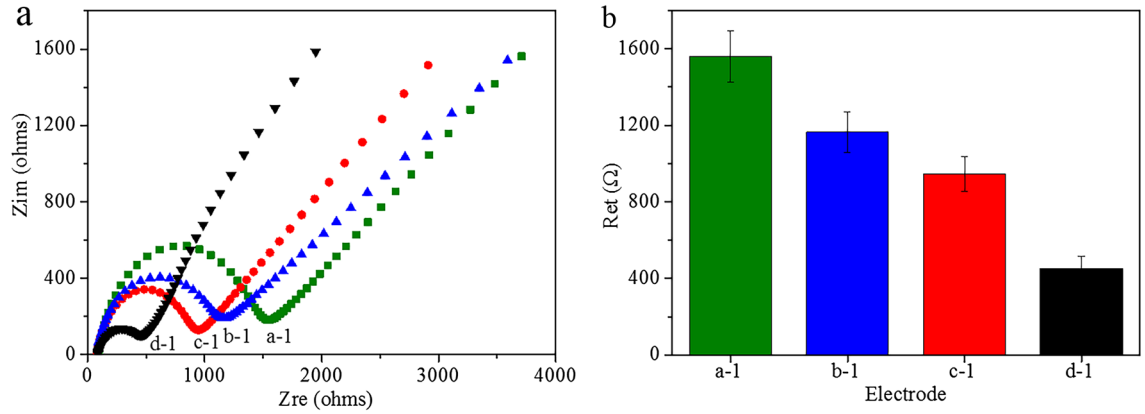

Figure 2. (**a**) Nyquist plots and (**b**) semicircle diameters from EIS characterization of electrodes modified with different materials in 0.01 M PBS (pH = 7.0) containing 5 mM $[Fe(CN)_6]^{3-/4-}$ and 0.1 M KCl: (a-1) GE, (b-1) GE-G-Chi-PtNP, (c-1) GE-G-Chi-AuNP, (d-1) GE-G-Chi-Au/PtNP. Error bar = RSD (n = 5).

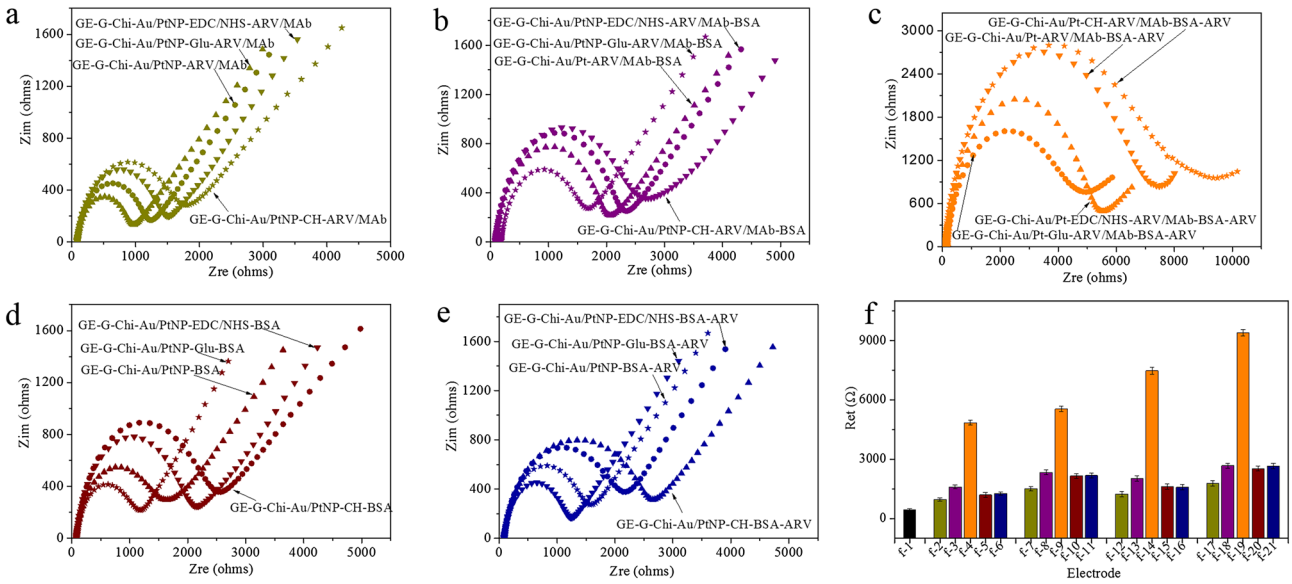

Figure 3. Nyquist plots for EIS characterization of electrodes after different modification steps in electrolyte (pH = 7.0) containing 5 mM $[Fe(CN)_6]^{3-/4-}$: (**a**) after ARV/MAb immobilization on GE-G-Chi-Au/PtNP, (**b**) after blocking with BSA, (**c**) after incubation with $10^{6.82}$ EID_{50} mL^{-1} ARV, (**d**) after blocking with BSA without ARV/MAb immobilization, (**e**) after incubation with $10^{6.82}$ EID_{50} mL^{-1} ARV without ARV/MAb immobilization; (**f**) R_{et} from EIS characterization of electrodes at different modification steps in electrolyte (pH = 7.0) containing 5 mM $[Fe(CN)_6]^{3-/4-}$: (f-1) GE-G-Chi-Au/PtNP, (f-2) GE-G-Chi-Au/PtNP-Glu-ARV/MAb, (f-3) GE-G-Chi-Au/PtNP-Glu-ARV/MAb-BAS, (f-4) GE-G-Chi-Au/PtNP-Glu-ARV/MAb-BAS-ARV, (f-5) GE-G-Chi-Au/PtNP-Glu-BAS, (f-6) GE-G-Chi-Au/PtNP-Glu-BAS-ARV, (f-7) GE-G-Chi-Au/PtNP-EDC/NHS-ARV/MAb, (f-8) GE-G-Chi-Au/PtNP-EDC/NHS-ARV/MAb-BSA, (f-9) GE-G-Chi-Au/PtNP-EDC/NHS-ARV/MAb-BSA-ARV, (f-10) GE-G-Chi-Au/PtNP-EDC/NHS-BSA, (f-11) GE-G-Chi-Au/PtNP-EDC/NHS-BSA-ARV, (f-12) GE-G-Chi-Au/PtNP-ARV/MAb, (f-13) GE-G-Chi-Au/PtNP-ARV/MAb-BSA, (f-14) GE-G-Chi-Au/PtNP-ARV/MAb-BSA-ARV, (f-15) GE-G-Chi-Au/PtNP-BSA, (f-16) GE-G-Chi-Au/PtNP-BSA-ARV, (f-17) GE-G-Chi-Au/PtNP-CH-ARV/MAb, (f-18) GE-G-Chi-Au/PtNP-CH-ARV/MAb-BSA, (f-19) GE-G-Chi-Au/PtNP-CH-ARV/MAb-BSA-ARV, (f-20) GE-G-Chi-Au/PtNP-CH-BSA, (f-21) GE-G-Chi-Au/PtNP-CH-BSA-ARV. Error bar = RSD (n = 5).

GE-G-Chi-Au/PtNP-Glu-ARV/MAb-BSA showed saturation beyond $10^{3.82}$ EID_{50} mL^{-1} ARV and a linear range of 0–$10^{3.82}$ EID_{50} mL^{-1} ARV; the linear regression equation of the calibration curve was expressed as R_{et} (Ω) = 765 lgEID_{50} mL^{-1} + 1464 with a correlation coefficient of $R^2 = 0.96175$, a low detection limit of $10^{0.63}$ EID_{50} mL^{-1} ARV (S/N = 3) and a quantification limit of $10^{1.15}$ EID_{50} mL^{-1} ARV (S/N = 10) (Fig. 4a,b). GE-G-Chi-Au/PtNP-EDC/NHS-ARV/MAb-BSA showed saturation beyond $10^{3.82}$ EID_{50} mL^{-1} ARV and a linear range of 0–$10^{3.82}$ EID_{50} mL^{-1} ARV; the linear regression equation of the calibration curve was expressed as R_{et} (Ω) = 829 lgEID_{50} mL^{-1} + 2406 with a correlation coefficient of $R^2 = 0.98785$, a low detection limit of $10^{0.48}$ EID_{50} mL^{-1} ARV (S/N = 3) and a

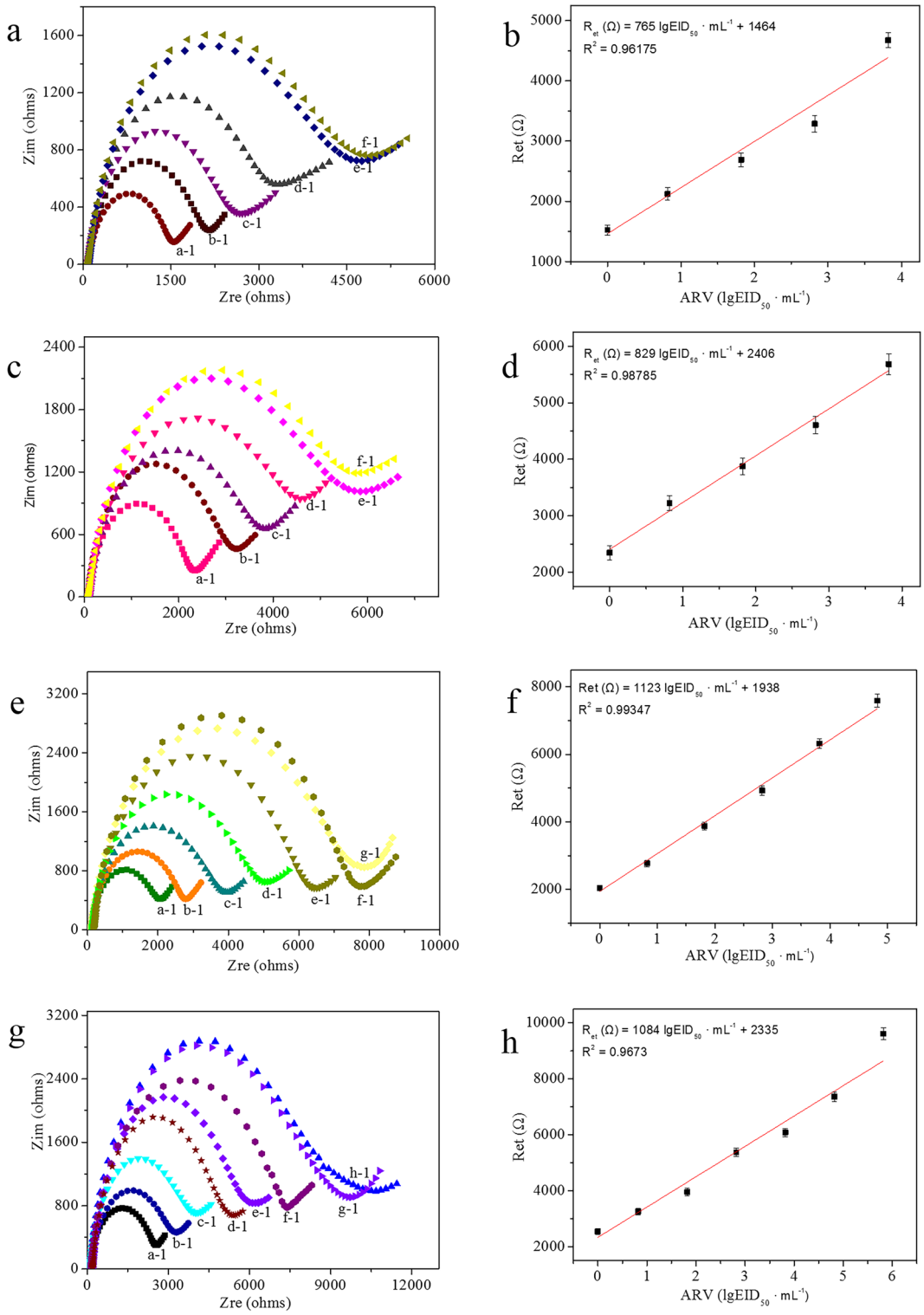

Figure 4. (**a**) Nyquist plots for different concentrations of ARV on GE-G-Chi-Au/PtNP-Glu-ARV/MAb-BSA; (**b**) Calibration curve of GE-G-Chi-Au/PtNP-Glu-ARV/MAb-BSA with different concentrations of ARV. Error bar = RSD (n = 5). (**c**) Nyquist plots for different concentrations of ARV on GE-G-Chi-Au/PtNP-EDC/NHS-ARV/MAb-BSA; (**d**) Calibration curve of GE-G-Chi-Au/PtNP-EDC/NHS-ARV/MAb-BSA with different concentrations of ARV. Error bar = RSD (n = 5). (**e**) Nyquist plots for different concentrations of ARV on GE-G-Chi-Au/PtNP-ARV/MAb-BSA; (**f**) Calibration curve for GE-G-Chi-Au/PtNP-ARV/MAb-BSA with different concentrations of ARV. Error bar = RSD (n = 5). (**g**) Nyquist plots for different concentrations of ARV on GE-G-Chi-Au/PtNP-CH-ARV/MAb-BSA; (**h**) Calibration curve for GE-G-Chi-Au/PtNP-CH-ARV/MAb-BSA with different concentrations of ARV. Error bar = RSD (n = 5). (a-1) 0, (b-1) $10^{0.82}$ EID_{50} mL^{-1} ARV, (c-1) $10^{1.82}$ EID_{50} mL^{-1} ARV, (d-1) $10^{2.82}$ EID_{50} mL^{-1} ARV, (e-1) $10^{3.82}$ EID_{50} mL^{-1} ARV, (f-1) $10^{4.82}$ EID_{50} mL^{-1} ARV, (g-1) $10^{5.82}$ EID_{50} mL^{-1} ARV, (f-1) $10^{6.82}$ EID_{50} mL^{-1} ARV.

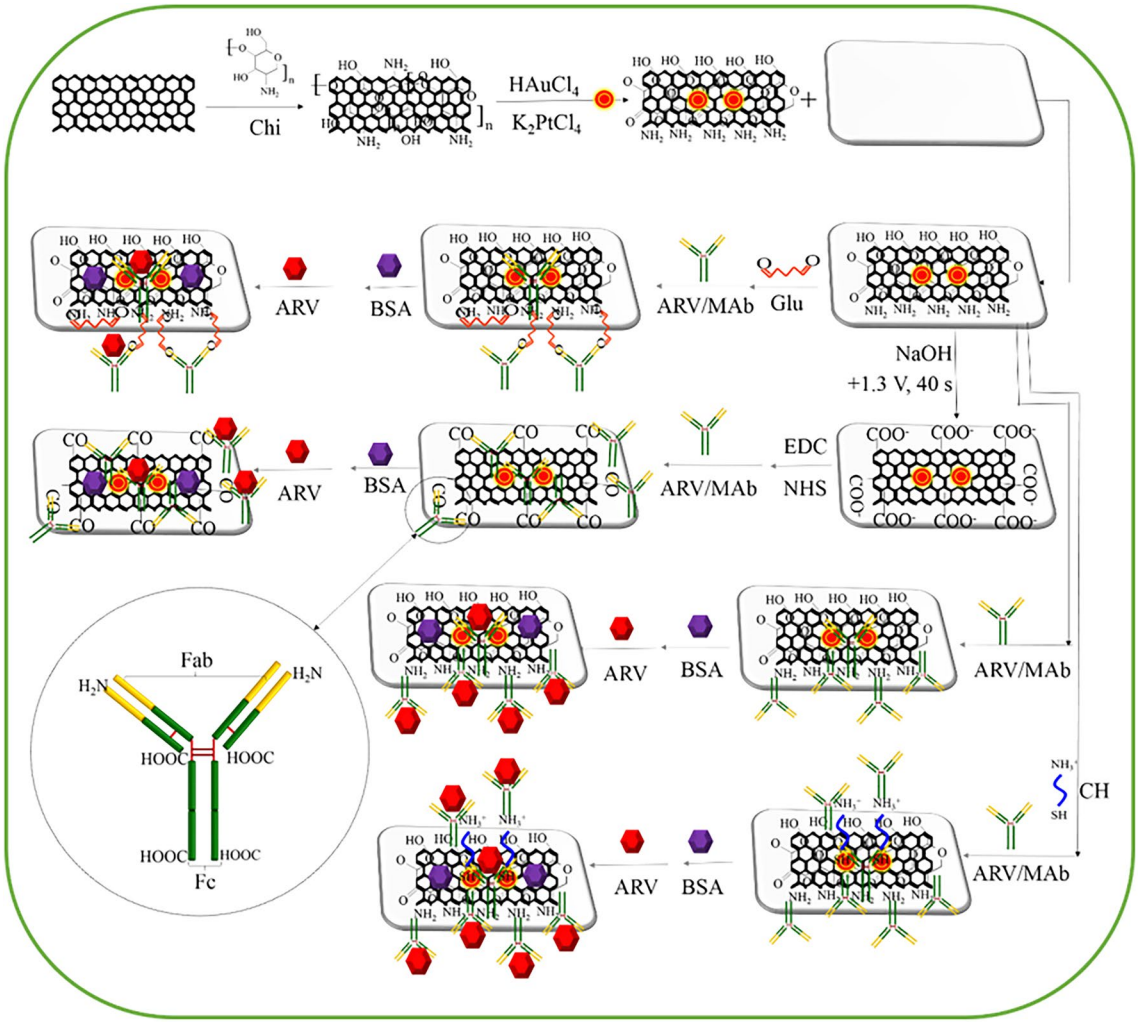

Figure 5. Schematic illustration of the electrochemical immunosensors.

quantification limit of $10^{1.00}$ EID_{50} mL^{-1} ARV (S/N = 10) (Fig. 4c,d). GE-G-Chi-Au/PtNP-ARV/MAb-BSA showed saturation beyond $10^{4.82}$ EID_{50} mL^{-1} ARV and a linear range of 0–$10^{4.82}$ EID_{50} mL^{-1} ARV; the linear regression equation of the calibration curve was expressed as R_{et} (Ω) = 1123 lgEID_{50} mL^{-1} + 1938 with a correlation coefficient of R^2 = 0.99347, a low detection limit of $10^{0.37}$ EID_{50} mL^{-1} ARV (S/N = 3) (Fig. 4e,f) and a quantification limit of $10^{0.89}$ EID_{50} mL^{-1} ARV (S/N = 10). GE-G-Chi-Au/PtNP-CH-ARV/MAb-BSA showed saturation beyond $10^{5.82}$ EID_{50} mL^{-1} ARV and a linear range of 0–$10^{5.82}$ EID_{50} mL^{-1} ARV; the linear regression equation of the calibration curve was expressed as R_{et} (Ω) = 1084 lgEID_{50} mL^{-1} + 2335 with a correlation coefficient of R^2 = 0.9673, a low detection limit of $10^{0.46}$ EID_{50} mL^{-1} ARV (S/N = 3) and a quantification limit of $10^{0.98}$ EID_{50} mL^{-1} ARV (S/N = 10) (Fig. 4g,h).

These results show that the sensitivities of the four immunosensors were slightly different, while saturation beyond the extended dynamic range of GE-G-Chi-Au/PtNP-CH-ARV/MAb-BSA was 10 times that of GE-G-Chi-Au/PtNP-ARV/MAb-BSA and 100 times those of GE-G-Chi-Au/PtNP-Glu-ARV/MAb-BSA and GE-G-Chi-Au/PtNP-EDC/NHS-ARV/MAb-BSA. These results were attributed to the different methods of ARV/MAb immobilization. ARV/MAb is a Y-shaped protein that consists of two light and two heavy chains linked by disulfide bonds, and ARV/MAb is monomeric (IgG) and contains the F_{ab} region and F_c region (Fig. 5). The F_{ab} region, which participates in antigen binding, consists of an amino end, while the F_c region, which is the stem of the Y shape, has a carboxyl end group[29,30]. The region (F_{ab} or F_c) of ARV/MAb attached to the electrode depended on immobilization strategy used. For GE-G-Chi-Au/PtNP-Glu-ARV/MAb-BSA, Glu was used as the coupling agent to connect amine groups on the surface of the electrode and amine groups (F_{ab} region) on ARV/MAb. The EDC/NHS-based immobilization strategy for GE-G-Chi-Au/PtNP-EDC/NHS-ARV/MAb-BSA activated carboxyl groups on the surface of the electrode and allowed NHS ester groups to act as intermediates leading to covalent attachment of the activated carboxyl groups with amino groups on the surface of the electrode present in the F_{ab} region on ARV/MAb. The antibodies in GE-G-Chi-Au/PtNP-ARV/MAb-BSA and GE-G-Chi-Au/PtNP-CH-ARV/MAb-BSA were immobilized onto the electrode via the tail end of the F_c region through covalent attachments between electrode surface amino groups and carboxyl groups on ARV/MAb, which resulted in accessibility for antigen binding because it was located in an orthogonal position. However, attachment of ARV/MAb onto

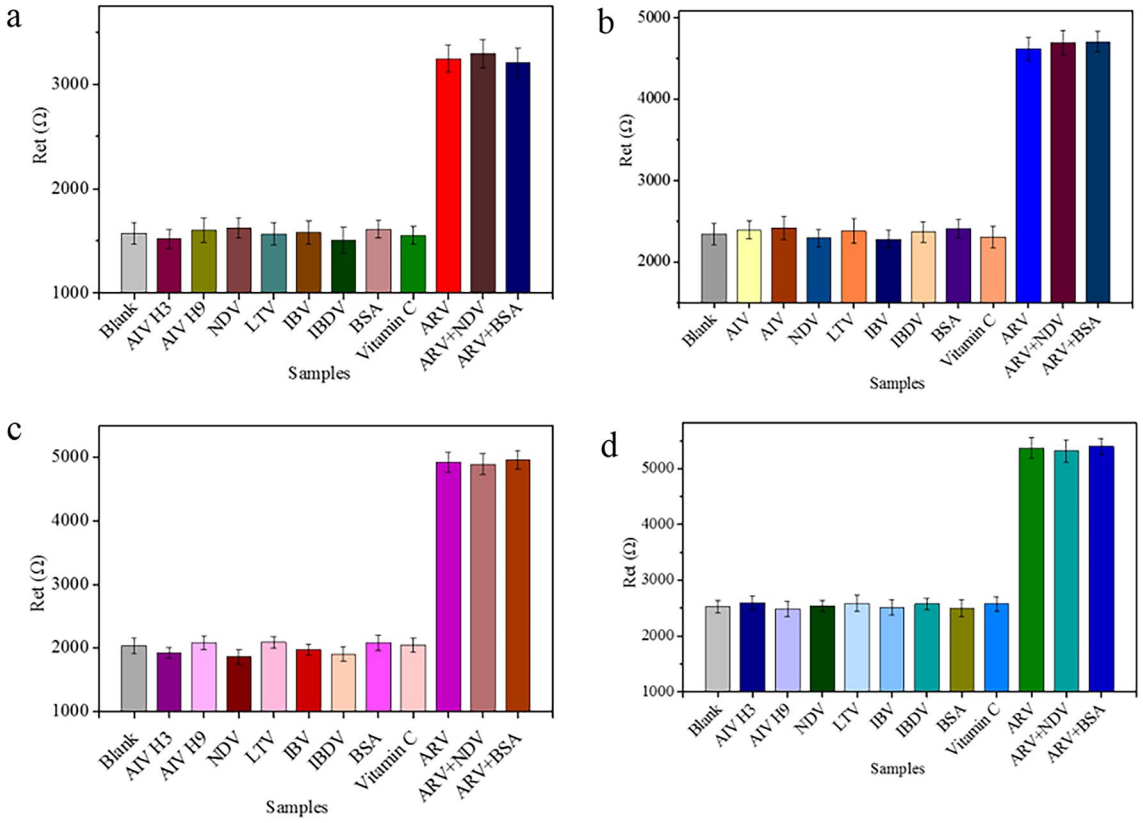

Figure 6. Specificity of the immunosensors toward the target (ARV) and other interfering substances. (**a**) GE-G-Chi-Au/PtNP-Glu-ARV/MAb-BSA, (**b**) GE-G-Chi-Au/PtNP-EDC/NHS-ARV/MAb-BSA, (**c**) GE-G-Chi-Au/PtNP-ARV/MAb-BSA, (**d**) GE-G-Chi-Au/PtNP-CH-ARV/MAb-BSA. Error bar = RSD (n = 5).

the electrode through the F_{ab} region led to a conformation providing difficult antibody–antigen binding because of steric hindrance. Therefore, GE-G-Chi-Au/PtNP-ARV/MAb-BSA and GE-G-Chi-Au/PtNP-CH-ARV/MAb-BSA showed higher saturation levels for ARV than GE-G-Chi-Au/PtNP-Glu-ARV/MAb-BSA and GE-G-Chi-Au/PtNP-EDC/NHS-ARV/MAb-BSA, because GE-G-Chi-Au/PtNP-ARV/MAb-BSA and GE-G-Chi-Au/PtNP-CH-ARV/MAb-BSA provided more active sites for antigen binding when ARV was present in high concentration. Although antibodies of GE-G-Chi-Au/PtNP-ARV/MAb-BSA and GE-G-Chi-Au/PtNP-CH-ARV/MAb-BSA were immobilized onto the electrode through the F_c region, GE-G-Chi-Au/PtNP-CH-ARV/MAb-BSA showed a higher saturation level for ARV because it featured more amine groups with which to adsorb more ARV/MAb.

The sensitivity of an immunosensor depends on changes in charge transfer resistance per unit change in ARV concentration per unit area. The four different immunosensors were modified with GE-G-Chi-Au/PtNP. So their electron transfer abilities on the surfaces of the four different immunosensors were similar. In the detection process, antigen–antibody complex formation resulted in similar changes in charge transfer resistance per unit change in ARV concentration per unit area, which provided similar sensitivities for the four different immunosensors. While the different strategies for antibody immobilization led to slight sensitivity differences among the four different immunosensors, GE-G-Chi-Au/PtNP-ARV/MAb-BSA showed the highest sensitivity among the four different immunosensors because ARV/MAb was immobilized on the surface of electrode by direct incubation (we did not use any non-conducting organics as linkers); ARV/MAb in the other three immunosensors was immobilized on the electrode surface with Glu, EDC/NHS and CH as linker, respectively. Glu, EDC/NHS and CH with poor electrical conductivities were attached to the electrodes, and the electron transfer abilities decreased, so the sensitivities of the immunosensors were decreased.

Selectivity, reproducibility and stability of the four immunosensors. The selectivity of GE-G-Chi-Au/PtNP-Glu-ARV/MAb-BSA, GE-G-Chi-Au/PtNP-EDC/NHS-ARV/MAb-BSA, GE-G-Chi-Au/PtNP-ARV/MAb-BSA and GE-G-Chi-Au/PtNP-CH-ARV/MAb-BSA played a crucial role in detecting target samples without separation. To evaluate the selectivities of the four different immunosensors, avian influenza virus H3 subtype (AIV H3, $10^{4.71}$ EID_{50} mL^{-1}), avian influenza virus H9 subtype (AIV H9, $10^{3.74}$ EID_{50} mL^{-1}), Newcastle disease virus (NDV, $10^{4.53}$ EID_{50} mL^{-1}), laryngotracheitis virus (LTV, $10^{3.86}$ EID_{50} mL^{-1}), infectious bronchitis virus (IBV, $10^{4.36}$ EID_{50} mL^{-1}), infectious bursal disease virus (IBDV, $10^{4.67}$ EID_{50} mL^{-1}), BSA (1.0 μg/mL) and vitamin C (1.0 μg/mL) were used as interfering substances. As shown in Fig. 6, the R_{et}s of the samples with the interfering substances were almost the same as that of the blank control, and the mixtures of ARV ($10^{2.82}$ EID_{50} mL^{-1}) with other possible interfering substances showed similar R_{et} values to those of ARV ($10^{2.82}$ EID_{50} mL^{-1}), indicating that GE-G-Chi-Au/PtNP-Glu-ARV/MAb-BSA, GE-G-Chi-Au/PtNP-EDC/NHS-ARV/

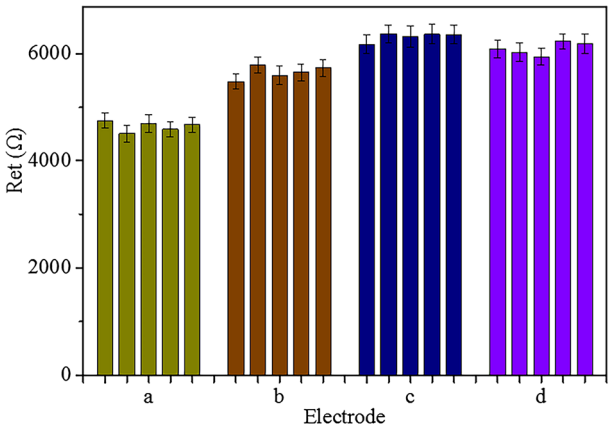

Figure 7. Reproducibility of the four immunosensors in the presence of $10^{3.82}$ EID_{50} mL^{-1} ARV (a) GE-G-Chi-Au/PtNP-Glu-ARV/MAb-BSA, (b) GE-G-Chi-Au/PtNP-EDC/NHS-ARV/MAb-BSA, (c) GE-G-Chi-Au/PtNP-ARV/MAb-BSA, (d) GE-G-Chi-Au/PtNP-CH-ARV/MAb-BSA. Error bar = RSD (n = 5).

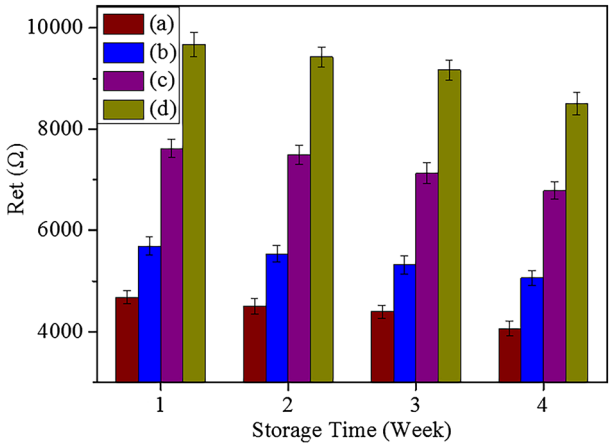

Figure 8. Long-term stability of the proposed immunosensors: (a) GE-G-Chi-Au/PtNP-Glu-ARV/MAb-BSA, (b) GE-G-Chi-Au/PtNP-EDC/NHS-ARV/MAb-BSA, (c) GE-G-Chi-Au/PtNP-ARV/MAb-BSA, (d) GE-G-Chi-Au/PtNP-CH-ARV/MAb-BSA.

MAb-BSA, GE-G-Chi-Au/PtNP-ARV/MAb-BSA and GE-G-Chi-Au/PtNP-CH-ARV/MAb-BSA had high selectivity for ARV detection.

The reproducibility of GE-G-Chi-Au/PtNP-Glu-ARV/MAb-BSA, GE-G-Chi-Au/PtNP-EDC/NHS-ARV/MAb-BSA, GE-G-Chi-Au/PtNP-ARV/MAb-BSA and GE-G-Chi-Au/PtNP-CH-ARV/MAb-BSA was investigated by EIS at the same concentration of $10^{3.82}$ EID_{50} mL^{-1} ARV. The results are shown in Fig. 7. The RSDs of GE-G-Chi-Au/PtNP-Glu-ARV/MAb-BSA, GE-G-Chi-Au/PtNP-EDC/NHS-ARV/MAb-BSA, GE-G-Chi-Au/PtNP-ARV/MAb-BSA and GE-G-Chi-Au/PtNP-CH-ARV/MAb-BSA were 2.04%, 2.12%, 1.30% and 1.92%, respectively, indicating that the four immunosensors have good reproducibility.

The long-term stability of the fabricated electrochemical immunosensors was further investigated by storing GE-G-Chi-Au/PtNP-Glu-ARV/MAb-BSA, GE-G-Chi-Au/PtNP-EDC/NHS-ARV/MAb-BSA, GE-G-Chi-Au/PtNP-ARV/MAb-BSA and GE-G-Chi-Au/PtNP-CH-ARV/MAb-BSA at 4 °C when not in use and then successively incubating them with ARV ($10^{5.82}$ EID_{50} mL^{-1}). As seen in Fig. 8, the R_{et}s remained at 91.72%, 90.39%, 93.07%, and 92.31% of the initial values when GE-G-Chi-Au/PtNP-Glu-ARV/MAb-BSA, GE-G-Chi-Au/PtNP-EDC/NHS-ARV/MAb-BSA, GE-G-Chi-Au/PtNP-ARV/MAb-BSA and GE-G-Chi-Au/PtNP-CH-ARV/MAb-BSA were stored at 4 °C for 4 weeks. The results indicated that the long-term stability of the four electrochemical immunosensors for ARV detection was acceptable.

Conclusions

In this work, four different antibody immobilization strategies (Glu as a coupling agent to connect amine groups on the surface of the electrode and amine groups present in ARV/Mab; EDC/NHS chemistry to activate carboxyl groups on the surface of the electrode for covalent attachment with amine groups present at the F_{ab} region on ARV/Mab; immobilization of ARV/MAb directly onto the amine group ending the electrode; and immobilization

of ARV/MAb directly onto the amine group ending the electrode after it was further modified with CH) were used to construct four different immunosensors (GE-G-Chi-Au/PtNP-Glu-ARV/MAb-BSA, GE-G-Chi-Au/PtNP-EDC/NHS-ARV/MAb-BSA, GE-G-Chi-Au/PtNP-ARV/MAb-BSA and GE-G-Chi-Au/PtNP-CH-ARV/MAb-BSA) to study the effect of immobilization strategy on the immunosensor performance. The EIS results showed that the extended dynamic range of GE-G-Chi-Au/PtNP-CH-ARV/MAb-BSA was 10 times that of GE-G-Chi-Au/PtNP-ARV/MAb-BSA and 100 times that of GE-G-Chi-Au/PtNP-Glu-ARV/MAb-BSA and GE-G-Chi-Au/PtNP-EDC/NHS-ARV/MAb-BSA, indicating that the immunosensors that immobilized the antibody via the F_c region obtained an extended dynamic response. In addition, the sensitivities, selectivities, reproducibilities and stabilities of the immunosensors were almost completely unaffected by the antibody immobilization strategies used in this work.

Methods

Bovine serum albumin (BSA), chloroauric acid tetrahydrate ($HAuCl_4{\cdot}4H_2O$) and chloroplatinic acid hexahydrate ($H_2PtCl_6{\cdot}6H_2O$) were procured from Sigma–Aldrich Chemical Co. (St. Louis, MO, USA.). Graphite powder (< 45 mm), potassium ferrocyanide ($K_4[Fe(CN)_6]$), potassium ferricyanide ($K_3[Fe(CN)_6]$), Glu, EDC, NHS, CH, H_2SO_4 and $KMnO_4$ were obtained from Guoyao Group Chemical Reagents Co., Ltd. (Shanghai, China).

Viruses and antibodies. ARV (S1133, China Institute of Veterinary Drug Control), AIV H3 (A/Duck/Guangxi/M20/2009, Guangxi Veterinary Research Institute), AIV H9 (A/Chicken/Guangxi/DX/2008, Guangxi Veterinary Research Institute), NDV (F48E9, China Institute of Veterinary Drug Control), LTV (ILT/13, China Institute of Veterinary Drug Control), IBV (Mass41, China Institute of Veterinary Drug Control) and IBDV (China Institute of Veterinary Drug Control) were collected and stored in a − 80 °C freezer in our laboratory prior to use. ARV/MAbs were prepared by our group[31].

Synthesis of G-Chi-Au/PtNP-ARV/MAbs. First, G was obtained by the Hummers method with slight modifications[32]. In short, 2.5 g $NaNO_3$ and 1.0 g graphite powder were added to 100 mL concentrated H_2SO_4 under continuous stirring and reacted at room temperature for 2 h. Then, the obtained mixture was cooled in an ice bath, 5 g $KMnO_4$ was slowly added under continuous stirring, and the mixture was kept for 24 h at 35 °C. Then, 100 mL ddH_2O was added to the mixture under continuous stirring, the mixture was kept for 3 h at 80 °C, and 300 mL ddH_2O was added. Subsequently, 6 mL 30% H_2O_2 was added, the mixture solution turned bright yellow, and many bubbles appeared. After continuous stirring for 3 h, the obtained solution was precipitated for 24 h at room temperature, the supernatant was decanted, 500 mL 0.5 mol/L HCl was added to the slurry, and the mixture was washed by centrifugation. Next, the obtained slurry was washed with ddH_2O until the pH of the supernatant was approximately 7.0. Then, 100 mL ddH_2O was added, and G oxide was obtained after ultrasonication for 2 h. The G oxide was heated to 95 °C in a water bath, 10 mL 1.0% $NaBH_4$ was added under continuous stirring, and the mixture was kept for 3 h, washed with ddH_2O three times, and dried in a vacuum drying oven at 90 °C for 8 h to obtain G.

Second, G-Chi was prepared according to our previous report[33]. Briefly, 0.05 mg Chi powder was added to 100 mL 1.0% (v/v) acetic acid solution under continuous stirring at room temperature and maintained for 0.5 h. Then, 100 mg of G was added, the mixture was continuously stirred for 24 h, and G-Chi was collected by centrifugation and washed with dd-H_2O.

Third, 1 mL 10 mmol/L $HAuCl_4$, 1 mL 10 mmol/L K_2PtCl_4 and 20 mL 1 mg/mL G-Chi solution were mixed together, and the mixture was stirred at room temperature for 3 h. Then, the mixture was heated to 80 °C under continuous stirring for 1 h to obtain the G-Chi-Au/PtNP nanocomposite.

Fabrication of the electrochemical immunosensor. The step-by-step fabrication of the electrochemical immunosensor is illustrated in Fig. 5. A gold electrode (GE) was polished with 1.0 μm, 0.3 μm, and 0.05 μm alumina polishing powders, rinsed with ddH_2O, and cleaned by sonication in ddH_2O, ethanol, and ddH_2O for 5 min each. Subsequently, the GE was dried by flushing with nitrogen gas.

Next, 8 μL of prepared G-Chi-Au/PtNP was dropped onto the surface of the clean GE and dried at room temperature, and G-Chi-Au/PtNP-GE was obtained. ARV/MAbs was immobilized onto G-Chi-Au/PtNP-GE by four different strategies: (1) G-Chi-Au/PtNP-GE was incubated with 10 μL of 5% Glu for 3 h and washed with PBS three times, and then 8 μL of 100 μg/mL ARV/MAbs was deposited onto G-Chi-Au/PtNP-Glu-GE and incubated at 4 °C for 8 h; (2) G-Chi-Au/PtNP-GE was anodized in 0.5 mol/L NaOH solution with a potential of + 1.3 V for 40 s to increase the number of –COOH groups on its surface. The anodized G-Chi-Au/PtNP-GE was incubated with 10 μL of solution that contained 50 mmol/L EDC and 30 mmol/L NHS in MES (pH 4.7) at room temperature for 1 h. –COOH groups were converted to amine-reactive NHS esters in this step to prepare for ARV/mAb immobilization. Then, after washing with PBS (pH 7.4) three times to remove the unreacted EDC/NHS, 8 μL 100 μg/mL ARV/MAbs was deposited onto the NHS-activated surface of G-Chi-Au/PtNP-EDC/NHS-GE, which was then incubated at 4 °C for 8 h; (3) 8 μL 100 μg/mL ARV/MAbs was deposited onto G-Chi-Au/PtNP-GE and incubated at 4 °C for 8 h without any further modification; and (4) G-Chi-Au/PtNP-GE was incubated with 10 μL 2 mg/mL CH at room temperature in the dark for 4 h and washed with PBS three times, after which 8 μL 100 μg/mL ARV/MAbs was deposited onto G-Chi-Au/PtNP-CH-GE, and the material was incubated at 4 °C for 8 h. All the electrodes with immobilized ARV/MAbs prepared via above four strategies were washed with PBS (pH 7.4) to remove physically adsorbed or excess ARV/MAbs, incubated with 1% BSA in 0.01 mol/L PBS (pH 7.4) at room temperature for 1 h to block the free active sites on the electrodes and washed three time with PBS (pH 7.4). The obtained immunosensors were denoted GE-G-Chi-Au/PtNP-Glu-ARV/MAb-BSA, GE-G-Chi-Au/

PtNP-EDC/NHS-ARV/MAb-BSA, GE-G-Chi-Au/PtNP-ARV/MAb-BSA and GE-G-Chi-Au/PtNP-CH-ARV/MAb-BSA, respectively, and stored at 4 °C until use.

Electrochemical analysis. The immunosensors were incubated with 8 µL of different concentrations of ARV at 37 °C for 30 min and washed with PBS (pH 7.4). Then, the sensors were subjected to EIS measurements in buffer containing 5.0 mM $K_3[Fe(CN)]_6$ and $K_4[Fe(CN)]_6$ in PBS (pH 7.4).

Data availability

All data generated or analyzed during this study are included in this article.

Received: 5 August 2022; Accepted: 20 December 2022
Published online: 23 December 2022

References

1. Li, J., Wang, C., Wang, W., Zhao, L. & Han, H. Dual-mode immunosensor for electrochemiluminescence resonance energy transfer and electrochemical detection of rabies virus glycoprotein based on Ru(bpy)32+-loaded dendritic mesoporous silica nanoparticles. *Anal. Chem.* **94**, 7655–7664 (2022).
2. Lee, T. H. *et al.* Development of an electrochemical immunosensor for detection of cardiac troponin I at the point-of-care. *Biosensors* **11**, 210 (2021).
3. Alves, N. J., Mustafaoglu, N. & Bilgicer, B. Oriented antibody immobilization by site-specific UV photocrosslinking of biotin at the conserved nucleotide binding site for enhanced antigen detection. *Biosens. Bioelectron.* **49**, 387–393 (2013).
4. Baniukevic, J. *et al.* Magnetic gold nanoparticles in SERS-based sandwich immunoassay for antigen detection by well oriented antibodies. *Biosens. Bioelectron.* **43**, 281–288 (2013).
5. Abolhasan, R. *et al.* Ultrasensitive and label free electrochemical immunosensor for detection of ROR1 as an oncofetal biomarker using gold nanoparticles assisted LDH/rGO nanocomposite. *Sci. Rep.* **11**, 14921 (2021).
6. Ortega, F. G. *et al.* Sandwich-type electrochemical paper-based immunosensor for claudin 7 and CD81 dual determination on extracellular vesicles from breast cancer patients. *Anal. Chem.* **93**, 1143–1153 (2021).
7. Biswas, S., Lan, Q., Xie, Y., Sun, X. & Wang, Y. Label-free electrochemical immunosensor for ultrasensitive detection of carbohydrate antigen 125 based on antibody-immobilized biocompatible MOF-808/CNT. *ACS Appl. Mater. Interfaces* **13**, 3295–3302 (2021).
8. Liu, X. *et al.* Label-free electrochemical immunosensor based on gold nanoparticle/polyethyleneimine/reduced graphene oxide nanocomposites for the ultrasensitive detection of cancer biomarker matrix metalloproteinase-1. *Analyst* **146**, 4066–4079 (2021).
9. Huang, J. *et al.* Electrochemical immunosensor with Cu(I)/Cu(II)-chitosan-graphene nanocomposite-based signal amplification for the detection of newcastle disease virus. *Sci. Rep.* **10**, 13869 (2020).
10. Du, X. *et al.* A label-free electrochemical immunosensor for detection of the tumor marker CA242 based on reduced graphene oxide-gold-palladium nanocomposite. *Nanomaterials* **9**, 1335 (2019).
11. Chen, Z. *et al.* A label-free electrochemical immunosensor based on a gold–vertical graphene/TiO_2 nanotube electrode for CA125 detection in oxidation/reduction dual channels. *Microchim. Acta* **189**, 257 (2022).
12. Ehzari, H., Amiri, M. & Safari, M. Enzyme-free sandwich-type electrochemical immunosensor for highly sensitive prostate specific antigen based on conjugation of quantum dots and antibody on surface of modified glassy carbon electrode with core–shell magnetic metal-organic frameworks. *Talanta* **210**, 120641 (2020).
13. Chaudhary, M. *et al.* Graphene oxide based electrochemical immunosensor for rapid detection of groundnut bud necrosis orthotospovirus in agricultural crops. *Talanta* **235**, 122717 (2021).
14. Wang, W. J., Chou, M. C., Lee, Y. J., Hsu, W. L. & Wang, G. J. A simple electrochemical immunosensor based on a gold nanoparticle monolayer electrode for neutrophil gelatinase-associated lipocalin detection. *Talanta* **246**, 123530 (2022).
15. Huang, Y., Wen, Q., Jiang, J. H., Shen, G. L. & Yu, R. Q. A novel electrochemical immunosensor based on hydrogen evolution inhibition by enzymatic copper deposition on platinum nanoparticle-modified electrode. *Biosens. Bioelectron.* **24**, 600–605 (2008).
16. Choosang, J., Khumngern, S., Thavarungkul, P., Kanatharana, P. & Numnuam, A. An ultrasensitive label-free electrochemical immunosensor based on 3D porous chitosan–graphene–ionic liquid–ferrocene nanocomposite cryogel decorated with gold nanoparticles for prostate-specific antigen. *Talanta* **224**, 121787 (2021).
17. Seidi, F., Reza Saeb, M., Huang, Y., Akbari, A. & Xiao, H. Thiomers of chitosan and cellulose: Effective biosorbents for detection, removal and recovery of metal ions from aqueous medium. *Chem. Rec.* **21**, 1876–1896 (2021).
18. Huang, L., Huang, W., Shen, R. & Shuai, Q. Chitosan/thiol functionalized metal–organic framework composite for the simultaneous determination of lead and cadmium ions in food samples. *Food Chem.* **330**, 127212 (2020).
19. Shen, Y., Shen, G. & Zhang, Y. Label-free electrochemical immunosensor based on ionic liquid containing dialdehyde as a novel linking agent for the antibody immobilization. *ACS Omega* **3**, 11227–11232 (2018).
20. Shen, Y. *et al.* A simple and sensitive electrochemical immunosensor based on thiol aromatic aldehyde as a substrate for the antibody immobilization. *Talanta* **141**, 288–292 (2015).
21. Halámek, J., Hepel, M. & Skládal, P. Investigation of highly sensitive piezoelectric immunosensors for 2,4-dichlorophenoxyacetic acid. *Biosens. Bioelectron.* **16**, 253–260 (2001).
22. Situ, C., Wylie, A. R. G., Douglas, A. & Elliott, C. T. Reduction of severe bovine serum associated matrix effects on carboxymethylated dextran coated biosensor surfaces. *Talanta* **76**, 832–836 (2008).
23. Johari-Ahar, M. *et al.* An ultra-sensitive impedimetric immunosensor for detection of the serum oncomarker CA-125 in ovarian cancer patients. *Nanoscale* **7**, 3768–3779 (2015).
24. Puertas, S. *et al.* Improving immunosensor performance through oriented immobilization of antibodies on carbon nanotube composite surfaces. *Biosens. Bioelectron.* **43**, 274–280 (2013).
25. Zhu, Q. *et al.* Highly selective and sensitive detection of glutathione over cysteine and homocysteine with a turn-on fluorescent biosensor based on cysteamine-stabilized CdTe quantum dots. *Spectrochim. Acta A Mol. Biomol. Spectrosc.* **267**, 120492 (2022).
26. Zhang, Y., Li, Y., Wu, W., Jiang, Y. & Hu, B. Chitosan coated on the layers' glucose oxidase immobilized on cysteamine/Au electrode for use as glucose biosensor. *Biosens Bioelectron.* **60**, 271–276 (2014).
27. Onda, K., Nakayama, M., Fukuda, K., Wakahara, K. & Arakai, T. Cell impedance measurement by Laplace transformation of charge or discharge current–voltage. *J. Electrochem. Soc.* **153**, A1012–A1018 (2006).
28. Park, J. Y. *et al.* (R)-lipo-diaza-18-crown-6 self-assembled monolayer as a selective serotonin receptor. *Anal. Chem.* **81**, 3843–3850 (2009).
29. Mimura, Y., Ashton, P. R., Takahashi, N., Harvey, D. J. & Jefferis, R. Contrasting glycosylation profiles between F_{ab} and F_c of a human IgG protein studied by electrospray ionization mass spectrometry. *J. Immunol. Methods* **326**, 116–126 (2007).
30. Mahan, A. E. *et al.* A method for high-throughput, sensitive analysis of IgG F_c and F_{ab} glycosylation by capillary electrophoresis. *J. Immunol. Methods* **417**, 34–44 (2015).

31. Xie, Z. Q. *et al.* Preparation and identification of monoclonal antibody against reovirus S1733. *China Anim. Husb. Vet. Med.* **39**, 47–51 (2012).
32. Yu, H., Zhang, B., Bulin, C., Li, R. & Xing, R. High-efficient synthesis of graphene oxide based on improved hummers method. *Sci. Rep.* **6**, 36143 (2016).
33. Huang, J. *et al.* Silver nanoparticles coated graphene electrochemical sensor for the ultrasensitive analysis of avian influenza virus H7. *Anal. Chim. Acta* **913**, 121–127 (2016).

Acknowledgements
This research project was funded by the Guangxi Science and Technology Projects (AB21076004), Youth Science Fund Project in Guangxi (2020GXNSFBA297104) and Guangxi BaGui Scholars Program Foundation (2019A50).

Author contributions
J.L.H. and Z.X.X. designed and conceived the experiments; J.L.H., L.J.X. and S.S.L. performed the experiments; and J.L.H., T.T.Z., Y.F.Z., M.X.Z., S.W., M.L., Y.W., Q.F., Z.Q.X., X.W.D. and D.L. analyzed the data and contributed reagents/materials/analysis tools. All authors reviewed the manuscript.

Competing interests
The authors declare no competing interests.

Additional information
Correspondence and requests for materials should be addressed to Z.X.

Reprints and permissions information is available at www.nature.com/reprints.

Publisher's note Springer Nature remains neutral with regard to jurisdictional claims in published maps and institutional affiliations.